Fabrication, Self-Assembly, and Properties of Ultrathin AlN/GaN Porous Crystalline Nanomembranes: Tubes, Spirals, and Curved Sheets

Yongfeng Mei,[†,*] Dominic J. Thurmer,[†] Christoph Deneke,[†] Suwit Kiravittaya,[†] Yuan-Fu Chen,[†] Armin Dadgar,[‡] Frank Bertram,[‡] Barbara Bastek,[‡] Alois Krost,[‡] Jürgen Christen,[‡] Thomas Reindl,[§] Mathieu Stoffel,[†,§] Emica Coric,[†] and Oliver G. Schmidt[†]

[†]Institute for Integrative Nanosciences, IFW Dresden, Helmholtzstrasse 20, D-01069 Dresden, Germany, [‡]Fakultät für Naturwissenschaften, Institut für Experimentelle Physik, Otto-von-Guericke-Universität Magdeburg, Universitätsplatz 2, D-39106 Magdeburg, Germany, and [§]Max-Planck-Institut für Festkörperforschung, Heisenbergstrasse 1, D-70569 Stuttgart, Germany

ABSTRACT Ultrathin AlN/GaN crystalline porous freestanding nanomembranes are fabricated on Si(111) by selective silicon etching, and self-assembled into various geometries such as tubes, spirals, and curved sheets. Nanopores with sizes from several to tens of nanometers are produced in nanomembranes of 20−35 nm nominal thickness, caused by the island growth of AlN on Si(111). No crystal-orientation dependence is observed while releasing the AlN/GaN nanomembranes from the Si substrate indicating that the driving stress mainly originates from the zipping effect among islands during growth. Competition between different relaxation mechanisms is experimentally revealed for different nanomembrane geometries and well-described by numerical calculations. The cathodoluminescence emission from GaN nanomembranes reveals a weak peak close to the GaN bandgap, which is dramatically enhanced by electron irradiation.

KEYWORDS: nanomembrane · GaN · AlN · porous · nanotube · rolled-up

Freestanding AlN/GaN nanomembranes have gained considerable interest, recently, because of applications in flexible electronics,[1,2] photonics,[3,4] sensor devices,[5] and microelectromechanical systems (MEMS).[6−9] Exceptional properties of AlN/GaN nanomembranes are manifold, including wide bandgap emission and absorption, good thermal and electrical conductivities,[2] large piezoelectricity,[5] large elastic modulus,[8] and excellent biocompatibility.[10] Freestanding nanomembranes driven by strain can self-assemble into certain geometries[11,12] such as micro/nanotubes[11−13] and spirals;[14] which serve for potential applications in, for example, electronics,[15,16] mechanics,[14] fluidics,[17,18] and photonics.[19] It is challenging, however, to create AlN/GaN nanomembranes due to limitations in growing ultrathin crystalline layers with thicknesses below 50 nm while retaining etching selectivity. It has been shown previously that freestanding AlN/GaN films with thicknesses larger 100 nm can buckle and bend.[20−23]

Here, we demonstrate that ultrathin crystalline AlN/GaN nanomembranes grown on Si(111), can be released by the selective etching of the silicon substrate and self-assemble into tubes, spirals, and curved sheets. Interestingly, *nanoporous crystalline microtubes* with pore sizes ranging from several to several tens of nanometers are produced when the layer thicknesses are in the range of 20−35 nm due to initial island growth of AlN on Si(111). During strain−relaxation, there is no particular dependence on crystal-orientation, suggesting that the driving stress mainly originates from the zipping effect among islands during growth. The competing relaxation mechanisms in nanomembranes with hundreds of nanometer width are experimentally investigated and explained by detailed simulations. The cathodoluminescence study shows that the photoemission close to the GaN bandgap from the ultrathin GaN layer can be dramatically enhanced by electron irradiation. These results suggest that shaped nanomembranes out of porous AlN/GaN are possible candidates for applications in for example, molecular separation[24] or artificial blood capillaries.[25]

RESULTS AND DISCUSSION

We first investigate the surface morphology of AlN films with various thicknesses (less than 50 nm) in order to determine the growth conditions allowing us to obtain

*Address correspondence to y.mei@ifw-dresden.de.

Received for review December 10, 2008 and accepted June 16, 2009.

Published online June 24, 2009.
10.1021/nn900580j CCC: $40.75

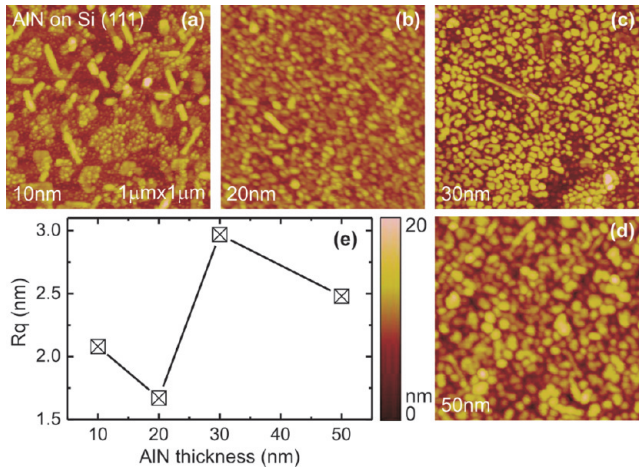

Figure 1. Surface morphologies of ultrathin AlN layers with various thicknesses of (a) 10, (b) 20, (c) 30, and (d) 50 nm grown on Si(111) checked by AFM; (e) surface roughness as a function of AlN layer thickness, analyzed from panels a−d.

continuous epitaxial films. After deposition of a 10 nm thick AlN film (Figure 1a) a mixture of small dots and rods, which do not coalesce, is observed. In contrast, a rather continuous epitaxial film is obtained after deposition of a 20 nm thick AlN film (Figure 1b). When the AlN films become thicker (as in Figure 1c,d: 30 and 50 nm, respectively), the size of the crystalline grains increases. The sample roughness stays within the same range for the different film thicknesses considered here (Figure 1(e)). As schematically shown in Figure 2a, after removal of the sacrificial layer (here Si), the AlN/GaN layer spontaneously forms into microtubes (Figure 2b) due to a strain gradient in the bilayer as discussed later.

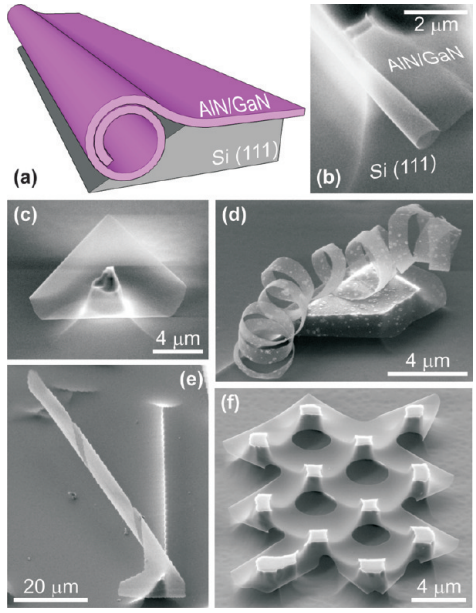

Figure 2. (a) A schematic diagram illustrating the shaping of an AlN/GaN nanomembrane into a microtube on Si(111) by etching away the sacrificial Si underneath; (b) an SEM image of a rolled-down AlN/GaN microtube on Si(111). Other types of shaped AlN/GaN nanomembranes: (c) a single curved sheet from a mesa structure, (d and e) spirals, and (f) a curved sheet from a defined hole array.

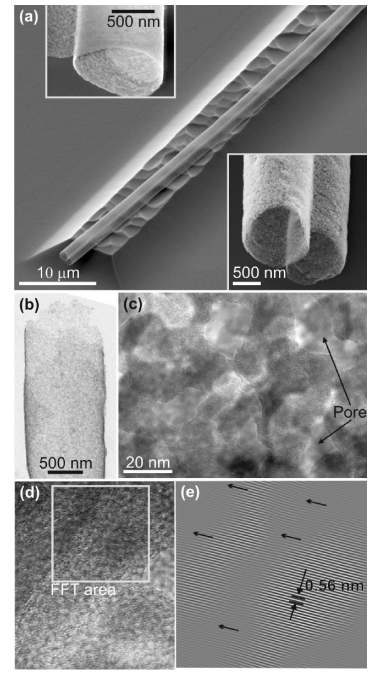

Figure 3. (a) An SEM image of two microtubes rolled from a striped AlN nanomembrane (20 nm thick) with a high aspect ratio on Si(111). The lower inset shows an enlarged SEM image of the open end in panel a, while the upper inset displays an SEM image of a pure AlN microtube with a layer thickness of 30 nm; (b) a TEM image of a selected AlN microtube having a layer thickness of 20 nm; (c) an enlarged TEM image showing the pores existing in the tube wall; (d and e) a high-resolution TEM image revealing the crystal structure of the rolled-up AlN membrane.

It should be mentioned here, that we use the AlN layers as a seeding layer for growing GaN layers on Si(111).[26] By varying the geometry of the defined pattern, freestanding AlN/GaN nanomembranes can also be shaped into curved sheets (Figure 2c,f) or spirals (Figure 2d,e), which has been systematically studied previously for other material systems.[27] A freestanding 20 nm thick AlN nanomembrane released from a high aspect ratio rectangular mesa rolls up into two microtubes with a diameter of about 1 μm, as shown in Figure 3a. An enlarged SEM image (lower inset) reveals its porous character. It is noted that the porous feature was also observed in our GaN/AlN nanomembranes (not shown). For comparison, a microtube from a 30 nm thick nanomembrane was also studied, which confirms that pores also exist in the tube walls (upper inset). The pores, however, are smaller in 30-nm-thick nanomembranes than those in 20-nm-thick films (see enlarged SEM images in the Supporting Information, Figures 2 and 3). Comprehensive transmission electron microscopy (TEM) was conducted to study the pores in more detail and to investigate the crystalline quality of these ultrathin shaped nanomembranes. Figure 3b shows an overview TEM image of a selected microtube created by a nominal 20 nm thick AlN nanomembrane. A magnified image (Figure 3c) clearly resolves the pores with a size of 10−20 nm. Furthermore, the grains of the

rolled-up nanostructure can be observed in the TEM images of Figure 3b,c. The grains form a dense network. From literature[26,28] as well as from the obtained diffraction image of flat areas of the tube (not shown), a highly textured growth in the ⟨0001⟩ direction is expected and observed. To investigate the structure and the crystal quality of the grown and released AlN membrane forming the rolled-up tube, high-resolution TEM (HRTEM) was carried out on several positions. In Figure 3d a HRTEM image near the {001} pole position is shown. Two neighboring grains, the grain boundary as well as a pore in the AlN membrane can be observed. In the center of the image clear lattice fringes are visible indicating a similar lattice alignment of the two grains. To verify the crystal quality and the lattice spacing, a fast Fourier transformed (FFT) filtered image of the region is depicted in Figure 3d. The measured distance of two lattice fringes (0.56 nm) agrees reasonable well with the expected distance of the lattice spacing of the d_{100} lattice planes (2×0.27 nm).[29] Furthermore, the coalescing single grains can be clearly distinguished by the grain boundary of 2−3 nm between grains. The TEM as well as HRTEM results not only verify the expected strong texture of the grains in the ⟨0001⟩-growth direction but also imply a preferred crystal orientation of neighboring grains separated by low angle grain boundaries. Normally, such boundaries are formed by a dislocation network and several dislocations in the crystal structure between grains are indicated by the arrows.

It is well-known that a large lattice mismatch of 19% exists between AlN(0001) and Si(111), which results in island formation during the initial growth stage.[28] It was reported that AlN films grown on Si(111) with a thickness of up to 20 nm causes formation of isolated islands on the surface.[28] In our experiments, for the deposition of 10 nm thick AlN, no film was found on the sample surface after removing the sacrificial layer, indicating that layers thinner than roughly 10 nm are not continuous (*i.e.*, coalescent). We found that 20 nm thick AlN films are continuous but porous, directly reflecting the partial coalescence of neighboring islands, which produce the porous structures. The technique for releasing nanomembranes therefore not only offers a method to fabricate porous nanomembranes in view of practical applications,[24,25] but can also help to understand the initial seed growth of epitaxial layers.[28,30]

It is well-known that stress can drive nanomembranes into certain shapes,[31] such as tubes[11−13] or wrinkled channels.[17,32] Curled structures form due to a pronounced strain gradient within the layers. For high quality epitaxial layers, the strain gradient is usually generated by the lattice mismatch within a bilayer of two different materials, and the magnitude of the strain can be well tuned by changing the composition of at least one of the layers.[33] In ref 34, a strain gradient was created in a single material film, in which the upper part of the layer relaxes because it is grown beyond the critical thickness for plastic relaxation.[34] More recently, a new rolled-up method was developed employing polymers as sacrificial layers and inorganic films as functional layers. The polymer sacrificial layer was removed by a solvent (such as acetone) and the inorganic layer forms into tubular structures.[5] In this case, the difference in the thermal expansion coefficients between the polymer and deposited inorganic layers is believed to be mainly responsible for the strain gradient generation. When AlN is grown on Si(111), the island growth occurs up to a deposition thickness of 10 nm. For thicker layers, the islands become larger and eventually coalesce generating tensile stress known as a "zipping" mechanism.[28,35] Beyond this critical thickness, no further tensile stress is created since no new islands form. This effect creates a strain gradient in the AlN/GaN layers, where the lower part close to the islands experiences tensile strain and the upper part close to the surface has little or no strain. These assumptions are confirmed in our experiments, since all the curved structures roll downward toward the substrate surface as shown in Figure 2b−f.

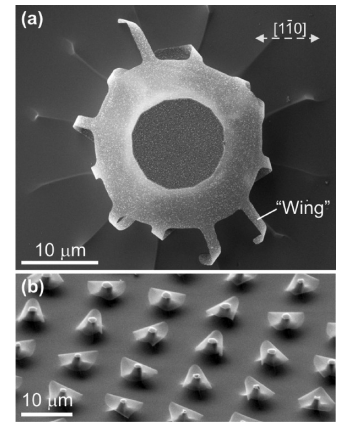

Figure 4. Scanning electron microscope images of curled AlN nanomembranes with the layer thickness of 30 nm on Si(111) after etching (a) clock and (b) mesa-shaped structures.

To exclude other possibilities for the generation of the strain gradient, two types of patterns were defined: a clock shape as shown in Figure 4a and a simple array of mesa structures as in Figure 4b. For pseudomorphic layer systems, the rolling usually proceeds along the soft crystal direction to minimize the total energy of the system.[11,12,33] If such a mechanism is dominant in the AlN/GaN layers, there would be six preferred rolling directions arising from the wurtzite structure. This symmetry would arise from the wurtzite crystal structure of the AlN/GaN film in its ⟨0001⟩ direction. Our structural analysis by TEM indicates a strongly textured but grainy material, which also could lift the six-folded symmetry of the AlN/GaN film. On the other hand, the evolution of the thin film growth observed in our AFM study could lead to an additional strain gradient caused by the overgrowth of the AlN porous structure by the GaN film. To clarify the presence of a preferred rolling direction as well as the presence of additional strain arising from the AlN/GaN film other than the island formation, clock-shaped and triangle-shaped mesas with arms were defined on the surface. After release of the film from these mesas, however, there appears to be no pronounced directional-dependent rolling in either the clock- nor in the mesa-shaped patterns (see Figure 4a,b). In the clock-shaped pattern, some "wings" have not bent down like others but this effect is attributed

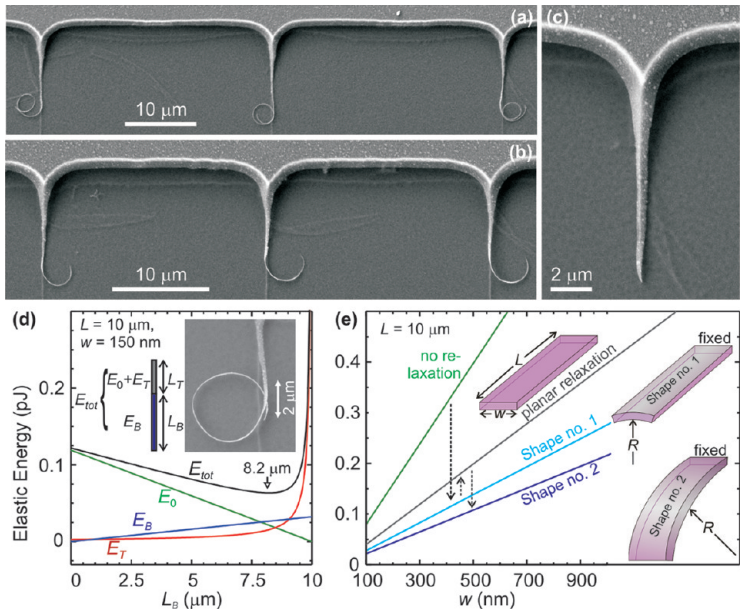

Figure 5. (a−c) SEM images of freestanding AlN/GaN nanomembranes with different width *w*. Smaller width has more number of spiral rotation as shown in panel a. All rolled nanomembrane is shown with a twisting of about 90°. (d) The calculated elastic energy contribution from the torsion part and the bending part. The torsion of the membrane limits the rolling distance. Origin of torsion is due to the preferential rolling on the long edge at the beginning. Inset of panel d shows a magnified SEM image of a spiral; torsion part with the length of ∼2 μm is observed. (e) The calculated elastic energy as a function of membrane width for different shapes (no relaxation, planar relaxation, shape no. 1, and shape no. 2). Vertical dash line and arrows describe the shape evolution pathway of observed spiral shapes. (See text for more detail.)

rather to fluid dynamics during the etching and/or critical drying process than to any crystal anisotropy. In the mesa array, the freestanding nanomembranes are curled down randomly. Since there appears to be no preferred shape of the islands as well as no preferred connection between the islands, we believe that the zipping mechanism contributes mostly to the strain gradient in the AlN/GaN curved nanomembranes.

To facilitate a deeper insight into the strain relaxation of freestanding nanomembranes, AlN/GaN (10 nm/10 nm in thickness) stripes with width *w* (100−1000 nm) and length *L* (10−20 μm) are realized by means of optical lithography and wet chemical etching as described above. Figure 5a−c display SEM images of the freestanding nanomembrane stripes after relaxation. For the patterns with a small width (hundreds of nanometers; for example ∼150 nm) as shown in Figure 5 panels a and b, spiral shapes are formed. The strain gradient originates from the morphological evolution during film growth and causes a "bending-down" of the structures. After a certain underetching length, the stripes are twisted by ∼90° due to interaction with the substrate surface. In contrast, the freestanding nanomembranes with larger widths of ∼1 μm (one typical SEM image shown in Figure 5c) show no such rolling into a spiral shape. In the following we discuss these two phenomena: (1) the roll-up of narrow stripes (roughly 100−500 nm wide), which ceases before the loose end reaches the fixed end; (2) no roll-up for wide stripes (roughly 500−1000 nm wide).

The cease of the roll-up mechanism by twisting the stripes is quantitatively described by a total elastic strain energy calculation shown in Figure 5d. First, the initial strain gradient (0.64%) is estimated from the obtained spiral diameter (∼3.4 μm).[36] The stripe of length *L* is divided into 2 parts, that is, a twisted part with a length L_T and a rolled part with a length L_B. The elastic energy of the first part has two contributions from the unrelaxed layer (E_0) and the torsion part (E_T). The unrelaxed strain is proportional to the length $E_0 \propto L_T$. Here we analytically calculate the torsion energy[37] assuming a constant torsion angle per unit length of $\pi/(2L_T)$ and we obtain the torsion energy $E_T \propto 1/L_T$. The second part of the stripe rolls up and the elastic energy is relaxed into E_B, which is obtained by minimizing this energy in cylindrical coordinates.[38] Because of the relaxation by rolling into a spiral shape, the elastic energy is reduced to 27% of the initial elastic energy, and this bending energy is proportional to the bending length $E_B \propto L_B$. By considering a rectangular stripe with width *w* of 150 nm and total length *L* of 10 μm, the total elastic energy is minimized at a bending distance of 8.2 μm. This is consistent with the experimental result shown in the inset of Figure 5d. Note that the twisting part of the stripe has a length of ∼2 μm. By changing the total length *L* without changing the stripe width, the calculation shows that the equilibrium bending length L_B increases while L_T is almost constant (at ∼2 μm for this condition).

Our above total elastic energy minimization cannot explain the nonspiral feature of the free-standing AlN/GaN nanomembrane with a larger width ($w > 500$ nm) as shown in Figure 5c. However, by considering the elastic energy for different shapes as a function of stripe width, we can theoretically explain this nonspiral phenomenon (see Figure 5e). In this figure, the total elastic energy of shape no. 1 is numerically calculated by assuming that the curvature ($1/R$) varies linearly from the equilibrium value at the free end to zero at the fixed end. The obstruction of the spiral formation can be explained as follows: During the initial underetching process, the unrelaxed film can gradually release the energy by bending downward, and it prefers to bend along the long edge (shape no. 1 in Figure 5e) because of its lower energy configuration. To further release the elastic energy after the underetching process is complete, the nanomembrane with shape no. 1 has to transform to the planar relaxation and then form into shape no. 2. This means that there is an energy barrier in this process (dashed line and arrow in Figure 5e). For a small width *w*, the energy barrier is small; therefore, a shape instability due to fluidic dynamics during etching can easily induce the stripe transformation from shape no. 1 to shape no. 2. In contrast, the stripe with

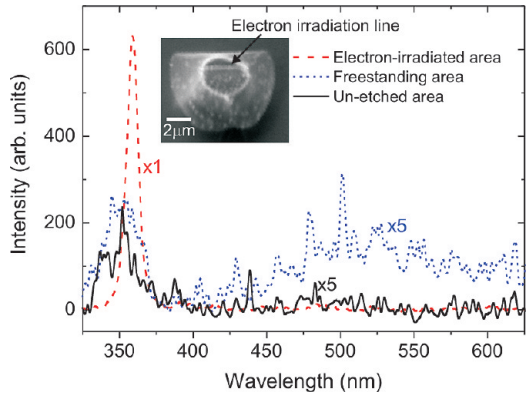

Figure 6. CL spectra of an ultrathin AlN/GaN layer (thickness: AlN 15 nm; GaN 20 nm) in unetched, freestanding, and electro-irradiated areas, measured at 4.2 K.

a larger width might not be able to overcome the barrier and therefore stays in the configuration of the shape no. 1. It is noted that at this considered length, the torsion energy is relatively small and negligible compared to the bending energy.

The optical properties of AlN/GaN nanomembranes were investigated by cathodoluminescence (CL) at 4.2 K, which is often used to characterize wide bandgap semiconductors.[39−41] The sample investigated consists of 20 nm GaN/15 nm AlN//Si(111) substrate. As presented in Figure 6, several areas of the sample were measured: an unetched area, a freestanding area, and an electron-irradiated area. The electron-irradiated area was generated by an electron beam when recording the CL spectra in the SEM. A nanomembrane containing one electron irradiation line is shown in the inset of Figure 6. In the unetched area, bandgap related emission of GaN at ~350 nm (~3.54 eV) is observed (black solid line). In the freestanding area, defects were generated in the nanomembranes by the etching process, which leads to a broad visible emission band observed at around ~500 nm (blue dotted line).[42] In both the unetched and freestanding areas, the bandgap emission is very weak. However, when the layer is irradiated by an electron beam while measuring, the bandgap emission is enhanced by 1 order of magnitude compared to the nonirradiated. In ZnO materials, Hui *et al.* have reported an enhanced ultraviolet (UV) emission after electron-beam irradiation when the layer is coated by an AlO_x layer.[40] Xie *et al.*[41] suggest that such enhancement could be due to the desorption of absorbed water from the ZnO. Here, the layers were grown at a high temperature (1050 °C) and should be well-crystallized; therefore, recrystallization of the GaN layers is excluded as a reason for the CL enhancement. We therefore believe that the desorption of water adsorbed during wet-chemical etching in such ultrathin porous nanomembranes can be responsible for the improved band-gap CL emission of GaN.

CONCLUSION

We have fabricated ultrathin, crystalline, porous AlN/GaN nanomembranes, which self-assemble into tubes, spirals, and curved sheets after selective etching of the underlying Si(111) substrate. Nanopores with sizes ranging from several to several tens of nanometers are produced in 20−35 nm thick nanomembranes due to the island growth of AlN on Si(111). The rolling direction does not depend on any particular crystal orientation, implying that the driving strain is mainly created by a so-called zipping effect due to island formation during growth. Competing relaxation processes in narrow nanomembranes are experimentally revealed for different structural geometries and explained by simulations. CL emission from a GaN nanomembrane originates from the GaN bandgap, and can be dramatically enhanced by electron irradiation due to desorption of adsorbed water.

EXPERIMENTAL DETAILS

The AlN/GaN samples were grown by metalorganic vapor phase epitaxy (MOVPE) using an Aixtron AIX 200/4 RF-S reactor. The (111) silicon substrates were chemically etched to remove the oxide layer and to produce a hydrogen-terminated surface. Prior to deposition of the AlN layer, the substrate was exposed to trimethylaluminum (TMAl) for 10 s in order to prevent the formation of a Si_xN_y layer. The AlN layer was then grown at 1050 °C using a mixture of TMAl and ammonia. Afterward, the GaN layer was deposited at the same temperature using trimethylgallium (TMGa) and ammonia. Different patterns were defined on the sample surface by photolithography and subsequent reactive ion etching using $SiCl_4$ gas.[43] The sacrificial silicon underneath the AlN/GaN layer was then selectively removed by a 1−3 min etching bath, in a solution consisting of HNO_3 (69%) and HF (50%) with a volume ratio of 10:1. For this particular concentration, the Si etching rate is around 3 μm per minute. We did not witness any obvious erosion effect on our AlN/GaN layers due to the etchant (see Supporting Information). A supercritical point dryer was adopted in the fabrication of shaped nanomembranes to avoid the structure collapsing due to the surface tension of the aqueous etchants. Since we observe rolling-down of the tubes, the AlN layer is the inner layer and the GaN layer is the outer layer. The morphology of the sample was investigated by a Zeiss NVision40 scanning electron microscope (SEM) and a FEI Tecnai T20 transmission electron microscope (TEM), while the surface morphology was characterized by a Veeco Dimension 3100 atomic force microscope (AFM) in tapping mode. The cathodoluminescence (CL) measurement at 4.2 K was performed in a homemade setup, based on a modified JEOL 6400 SEM.

Acknowledgment. We are grateful for the assistance from B. Eichler, S. Sieber, I. Mönch, V. A. Bolaños Quiñones, S. Baunack, and S. Harazim. B. Rellinghaus is acknowledged for access to the FEI T20 TEM. This work was financially supported by the BMBF (No. 03X5518).

Supporting Information Available: The etching rate of Si by the used etchant, as well as its erosion effect on AlN/GaN layers; high-resolution images of the insets in Figure 3a. This material is available free of charge *via* the Internet at http://pubs.acs.org.

REFERENCES AND NOTES

1. Ahn, J. H.; Kim, H. S.; Lee, K. J.; Jeon, S.; Kang, S. J.; Sun, Y. G.; Nuzzo, R. G.; Rogers, J. A. Heterogeneous Three-Dimensional Electronics by Use of Printed Semiconductor Nanomaterials. *Science* **2006**, *314*, 1754–1757.

2. Lee, K. J.; Meitl, M. A.; Ahn, J.-H.; Rogers, J. A.; Nuzzo, R. G. Bendable GaN High Electron Mobility Transistors on Plastic Substrates. *J. Appl. Phys.* **2006**, *100*, 124507.
3. Choi, Y.-S.; Hennessy, K.; Sharma, R.; Haberer, E.; Gao, Y.; DenBaars, S. P.; Meier, C. GaN Blue Photonic Crystal Membrane Nanocavities. *Appl. Phys. Lett.* **2005**, *87*, 243101.
4. Tamboli, A. C.; Haberer, E. D.; Sharama, R.; Lee, K. H.; Nakamura, S.; Hu, E. L. Room-Temperature Continuous-Wave Lasing in GaN/InGaN Microdisks. *Nat. Photonics* **2007**, *1*, 61–64.
5. Zimmermann, T; Neuburger, M.; Benkart, P.; Hernández-Guillén, F. J.; Pietzka, C.; Kunze, M.; Daumiller, I.; Dadgar, A.; Krost, A.; Kohn, E. Piezoelectric GaN Sensor Structures. *IEEE Electron Device Lett.* **2006**, *27*, 309–312.
6. Cleland, A. N.; Pophristic, M.; Ferguson, I. Single-Crystal Aluminum Nitride Nanomechanical Resonators. *Appl. Phys. Lett.* **2001**, *79*, 2070.
7. Foerster, Ch.; Cimalla, V.; Brueckner, K.; Lebedev, V.; Stephan, R.; Hein, M.; Ambacher, O. Processing of Novel SiC and Group III-Nitride Based Micro- and Nanomechanical Devices. *Phys. Status Solidi* **2005**, *202*, 671–676.
8. Yang, Z.; Wang, R. N.; Jia, S.; Wang, D.; Zhang, B. S.; Lau, K. M.; Chen, K. J. Mechanical Characterization of Suspended GaN Microstructures Fabricated by GaN-on-Patterned-Silicon Technique. *Appl, Phys. Lett.* **2006**, *88*, 041913.
9. Brueckner, K.; Niebelschuetz, F.; Tonisch, K.; Michael, S.; Dadgar, A.; Krost, A.; Cimalla, V.; Ambacher, O.; Stephan, R.; Hein, M. A. Two-Dimensional Electron Gas Based Actuation of Piezoelectric AlGaN/GaN Microelectromechanical Resonators. *Appl. Phys. Lett.* **2008**, *93*, 173504.
10. Stutzmann, M.; Garrido, J. A.; Eickhoff, M.; Brandt, M. S. Direct Biofunctionalization of Semiconductors: A Survey. *Phys. Status Solidi A* **2006**, *203*, 3424–3437.
11. Schmidt, O. G.; Eberl, K. Nanotechnology: Thin Solid Films Roll Up into Nanotubes. *Nature* **2001**, *410*, 168.
12. Prinz, V. Ya.; Seleznev, V. A.; Gutakovsky, A. K.; Chehovskiy, A. V.; Preobrazhenskii, V. V.; Putyato, M. A.; Gavrilova, T. A. Free-Standing and Overgrown InGaAs/GaAs Nanotubes, Nanohelices and Their Arrays. *Phys. E* **2000**, *6*, 828–831.
13. Mei, Y. F.; Huang, G. S.; Solovev, A. A.; Bermúdez Ureña, E.; Mönch, J. I.; Ding, F.; Reindl, T.; Fu, R. K. Y.; Chu, P. K.; Schmidt, O. G. Versatile Approach for Integrative and Functionalized Tubes by Strain Engineering of Nanomembranes on Polymers. *Adv. Mater.* **2008**, *20*, 4085–4090.
14. Bell, D. J.; Dong, L. X.; Nelson, B. J.; Golling, M.; Zhang, L.; Grützmacher, D. Fabrication and Characterization of Three-Dimensional InGaAs/GaAs Nanosprings. *Nano Lett.* **2006**, *6*, 725–729.
15. In, H. J.; Kumar, S.; Shao-Horn, Y.; Barbastathis, G. Origami Fabrication of Nanostructured, Three-Dimensional Devices: Electrochemical Capacitors with Carbon Electrodes. *Appl. Phys. Lett.* **2006**, *88*, 083104.
16. Meyer, G. J.; Dias, N. L.; Blick, R. H.; Knezevic, I. Magnetotransport in Nonplanar SiGe/Si Nanomembranes. *IEEE Trans. Nanotechnol.* **2007**, *6*, 446–450.
17. Mei, Y. F.; Thurmer, D. J.; Cavallo, F.; Kiravittaya, S.; Schmidt, O. G. Semiconductor Sub-micro-/nanochannel Networks by Deterministic Layer Wrinkling. *Adv. Mater.* **2007**, *19*, 2124–2128.
18. Thurmer, D. J.; Deneke, Ch.; Mei, Y. F.; Schmidt, O. G. Process Integration of Microtubes for Fluidic Applications. *Appl. Phys. Lett.* **2006**, *89*, 223507.
19. Kipp, T.; Welsch, H.; Strelow, Ch.; Heyn, Ch.; Heitmann, D. Optical Modes in Semiconductor Microtube Ring Resonators. *Phys. Rev. Lett.* **2006**, *96*, 077403.
20. Stonas, A. R.; MacDonald, N. C.; Turner, K. L.; Denbaars, S. P.; Hu, E. L. Photoelectrochemical Undercut Etching for Fabrication of GaN Microelectromechanical Systems. *J. Vac. Sci. Technol., B* **2001**, *19*, 2838–2841.
21. Takagaki, Y.; Sun, Y. J.; Brandt, O.; Ploog, K. H. Strain Relaxation in AlN/GaN Bilayer Films Grown on Gamma-$LiAlO_2$(100) for Nanoelectromechanical Systems. *Appl. Phys. Lett.* **2004**, *84*, 4756.
22. Zaus, E.; Hermann, M.; Stutzmann, M.; Eickhoff, M. Fabrication of Freestanding GaN Microstructures Using AlN Sacrificial Layers. *Phys. Status Solidi PRL* **2007**, *1*, R10−R12.
23. Strittmatter, R. P.; Beach, R. A.; McGill, T. C. Fabrication of GaN Suspended Microstructures. *Appl. Phys. Lett.* **2001**, *78*, 3226.
24. Striemer, C. C.; Gaborski, T. R.; McGrath, J. L.; Fauchet, P. M. Charge- and Size-based Separation of Macromolecules using Ultrathin Silicon Membranes. *Nature* **2007**, *445*, 749–753.
25. Wang, G. J.; Chen, C. L.; Hsu, S. H.; Chiang, Y. L. Bio-MEMS fabricated artificial capillaries for Tissue Engineering. *Microsyst. Technol.* **2005**, *12*, 120–127.
26. Kros, A.; Dadgar, A. GaN-based Optoelectronics on Silicon Substrates. *Mater. Sci. Eng., B* **2002**, *93*, 77–84.
27. Huang, M.; Boone, C.; Roberts, M.; Savage, D. E.; Lagally, M. G.; Shaji, N.; Qin, H.; Blick, R.; Nairn, J. A.; Liu, F. Nanomechanical Architecture of Strained Bilayer Thin Films: From Design Principles to Experimental Fabrication. *Adv. Mater.* **2005**, *17*, 2860–2864.
28. Liu, R.; Ponce, F. A.; Dadgar, A.; Krost, A. Atomic Arrangement at the AlN/Si(111) Interface. *Appl. Phys. Lett.* **2003**, *83*, 860.
29. Ott, H. Das Gitter des Aluminiumnitrids (AlN). *Z. Phys.* **1924**, *22*, 201.
30. Krost, A.; Dadgar, A.; Blasing, J.; Diez, A.; Hempel, T.; Petzold, S.; Christen, J.; Clos, R. Evolution of Stress in GaN Heteroepitaxy on AlN/Si(111): From Hydrostatic Compressive to Biaxial Tensile. *Appl. Phys. Lett.* **2004**, *85*, 3441.
31. Schmidt, O. G.; Schmarje, N.; Deneke, C.; Muller, C.; Jin-Phillipp, N. Y. Three-Dimensional Nano-objects Evolving from a Two-Dimensional Layer Technology. *Adv. Mater.* **2001**, *13*, 756–759.
32. Malachias, A.; Mei, Y. F.; Annabattula, R. K.; Deneke, C.; Onck, P. R.; Schmidt, O. G. Wrinkled-up Nanochannel Networks: Long-Range Ordering, Scalability, and X-ray Investigation. *ACS Nano* **2008**, *2*, 1715–1721.
33. Deneke, C.; Müller, C.; Jin-Phillipp, N. Y.; Schmidt, O. G. Diameter Scalability of Rolled-up In(Ga)As/GaAs Nanotubes. *Semicond. Sci. Technol.* **2002**, *17*, 1278–1281.
34. Songmuang, R.; Deneke, Ch.; Schmidt, O. G. Rolled-up Micro- and Nanotubes from Single-Material Thin Films. *Appl. Phys. Lett.* **2006**, *89*, 223109.
35. Hoffmann, R. W. The Mechanical Properties of Thin Condensed Films. *Phys. Thin Films* **1966**, *3*, 211.
36. Considered AlN/GaN film is assumed to have symmetric shape with 20 nm thick and isotopic elastic constants (Young modulus = 150 GPa, $\nu = 0.22$).
37. Chou, P. C.; Pagano, N. J. *Elasticity: Tensor, Dyadic, and Engineering Approaches*; Dover: New York, 1967.
38. Grundmann, M. Nanoscroll Formation from Strained Layer Heterostructures. *Appl. Phys. Lett.* **2003**, *83*, 2444.
39. Mei, Y. F.; Siu, G. G.; Fu, R. K. Y.; Chu, P. K.; Li, Z. M.; Zhai, J. P.; Liu, H. J.; Tang, Z. K.; Lai, C. W.; Ong, H. C. Visible Cathodoluminescence of 4 Å Single-Walled Carbon Nanotubes. *Appl. Phys. Lett.* **2005**, *87*, 213114.
40. Hui, K. C.; An, H. J.; Zhang, X. Y.; Xu, J. B.; Dai, J. Y.; Ong, H. C. Electron Beam Induced Light Emission and Charge Conduction Patterning in ZnO by Using an AlOx Layer. *Adv. Mater.* **2005**, *17*, 1960–1964.
41. Xie, R.; Sekiguchi, T.; Ishigaki, T.; Ohashi, N.; Li, D.; Yang, D.; Liu, B.; Bando, Y. Enhancement and Patterning of Ultraviolet Emission in ZnO with an Electron Beam. *Appl. Phys. Lett.* **2006**, *88*, 134103.
42. Kang, J.; Ogawa, T. Yellow Luminescence from Precipitates in GaN Epilayers. *Appl. Phys. A: Mater. Sci. Process.* **1999**, *69*, 631–635.
43. Zhang, L.; Ramer, J.; Brown, J.; Zheng, K.; Lester, L. F.; Hersee, S. D. Electron Cyclotron Resonance Etching Characteristics of GaN in $SiCl_4$/Ar. *Appl. Phys. Lett.* **1996**, *68*, 367.